Internet Journal of Society for Social Management Systems Vol.12 Issue 1 sms19-8001
ISSN: 2432-552X
ORIGINAL ARTICLE

Vegetation Recovery Monitoring using Satellite Imagery

Ryosuke Murai[1*], Masataka Takagi[2], Hiroaki Hanai

[1] Research Organization for Regional Alliances, Kochi University of Technology
185 Tosayamadacho-Miyanokuchi, Kami, Kochi, 782-8502, JAPAN

[2] School of Systems Engineering, Kochi University of Technology
185 Tosayamadacho-Miyanokuchi, Kami, Kochi, 782-8502, JAPAN

[*]E-mail: murai.ryosuke@kochi-tech.ac.jp

***Abstract*:** In recent years, vegetation has changed owing to various factors, such as global climate change, logging of artificial forests, and feeding damage caused by deer. In order to accurately measure changes in vegetation, it is necessary to study wide-area land cover changes for extended periods. Currently, satellite imagery can be acquired freely and easily. However, there are few artificial satellites that can be observed over a long period, with different performance. The aim of this study is mapping vegetation change for ten years (2018 from 2009) using multi-season satellite imagery. Sentinel-2, Landsat8/OLI, Landsat5/TM, and ALOS/AVNIR-2 imagery were used in this work. The multi-season refers to the defoliation start season, the defoliation season, and the leaf set season. The land cover was classified by machine learning with supervised data. A land cover classification map for 10 years was created using images of satellites with different spatial resolutions, observation wavelength bands, and numbers of bands. The land cover classification using Sentinel-2 data achieved an accuracy of 90.0%. Classification using Landsat 5 and ALOS data achieved an accuracy of 80.0% or higher. Using these different satellites, vegetation change maps were created from long-period land cover classification maps. Finally, in order to evaluate the effectiveness of the method, the vegetation change map was used to verify the correlation between environmental data and vegetation restoration; the obtained correlation coefficient was 0.824, indicating a strong correlation. The vegetation of the logging sites was restored to evergreen broad-leaved trees in areas with elevations less than 800 m of and to deciduous broad-leaved trees in areas with elevations higher than 800 m. The recovering period was 10 years at a 500 m elevation and over 18 years at a 1,000 m elevation. Vegetation logging sites were restored in less than 10 years where the surface lithology was phyllite.

Keywords: Remote sensing, satellite imagery, land cover classification, vegetation recovery

1. Introduction

In recent years, vegetation has changed owing to many factors, such as global climate change, logging of artificial forests, and feeding damage caused by deer. To understand these problems, it is necessary to observe these events and changes in vegetation over an extended period. Generally, artificial satellites are used to observe vegetation changes over a wide area

Received: 2019.07.31/ Accepted: 2019.11.27

Internet Journal of Society for Social Management Systems Published Date: 2019.12.20

for an extended period. Satellite images can be obtained freely and easily. However, although various satellites have been launched, their operating periods are too short to observe changes in vegetation（Figure 1). Figure 2 summarizes the observed wavelengths and spatial resolution of major satellites. Sentinel-2 is a European Earth observation satellite that has been in operation since 2015 and has 13 wavelength bands (four visible, six near-infrared, and three short-wavelength infrared). Sentinel-2 has 10 m spatial resolution, and high accurate land cover classification can be expected. Landsat is the Earth Observation Satellite of the United States Air and Space Agency (NASA), and it has performed continuous observation since 1972. The main spatial resolution of Landsat is 30 m. Landsat 8 has four visible bands, one near-infrared band, and three short wavelengths infrared bands. Compared to Landsat 8, Landsat 5 has fewer visible and short wavelength infrared bands. ALOS has a spatial resolution of 10 m and three visible bands, one of which in the near-infrared band. ALOS was operational from 2006 to 2011.

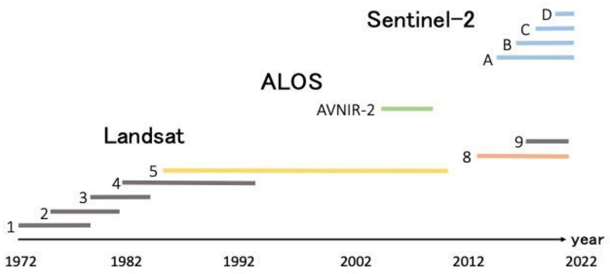

Figure 1 Operation period of various satellites

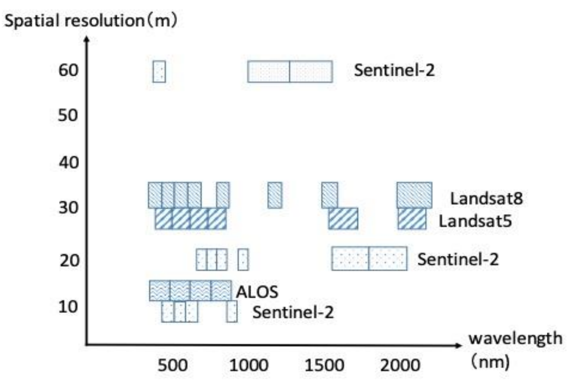

Figure 2 Observation wavelength and spatial resolution by satellite

1.1 Objectives

The purpose of this study is to enable long period observation of vegetation by combining data from different satellites. In this study, a land cover classification map for 10 years was created using satellite images with different spatial resolutions, observation wavelength bands, and numbers of bands. A vegetation change map was created from this long-period land cover classification map. Finally, in order to evaluate the effectiveness of the method, the vegetation change map was used to verify the correlation between environmental data and vegetation restoration.

2. Target area and usage data

2.1 Target area

The target area of this study is shown in Figure 3; it is a 36.20 × 27.15 km region that includes the cities of Otoyo-cho and Kami, which are located in the central part of Kochi Prefecture.

Figure 3 Target area

2.2 Usage data

This study used data from four types of satellites (Table 1). Satellite images were used for six of the ten years between 2009 and 2018. Table 2 shows the satellite images used in this study. Considering the seasonal change in vegetation, this study used three seasons (the defoliation start season, defoliation season, and leaf set season) for the classification for one year. The bands used for classification are shown in Table 3. A total of 13 bands were used from Sentinel-2: four visible bands, six near-infrared bands, and three short wavelengths infrared bands. Eight bands were used from Landsat 8: four visible bands, one near-infrared band, and three short wavelength infrared bands. A combination of six bands was used from Landsat 5 and ALOS: three visible bands of ALOS with a spatial resolution of 10 m, one ALOS near-infrared band, and two short wavelength infrared Landsat 5 bands with a spatial resolution of 30 m. In order to compensate for situations in which the number of bands was low, satellite images of six seasons were used when fusing Landsat 5 and ALOS. The case of fusing Landsat 5 and ALOS is represented by "Landsat5&ALOS".

Table 1 Used satellite and installed equipment

satelite	Installed sensor	
sentinel-2	Multispectral Imager	(MSI)
Landsat 8	Operational Land Imager	(OLI)
Landsat 5	Thematic Mapper	(TM)
ALOS	Advanced Visible and Near Infra-red Radiometer type 2	(AVNIR-2)

Table 2 Used satellite image

sentinel-2			Landsat 8			Landsat5&ALOS		
FY	time	Cloud Cover	FY	time	Cloud Cover	FY	time	Cloud Cover
2018	2018/05/24	0.57	2016	2016/07/19	7.07	2009 Landsat5	2006/11/13	5.00
	2018/04/19	0.00		2016/04/30	0.03		2009/09/02	15.00
	2017/11/05	0.28		2015/10/21	2.38		2009/04/11	7.00
2017	2017/09/26	2.30	2015	2015/09/19	9.34	2009 ALOS	2009/11/23	1.32
	2017/04/04	0.00		2015/04/30	0.03		2009/08/23	2.54
	2016/11/05	3.91		2014/11/03	10.22		2009/04/07	4.28
			2014	2014/10/18	12.09			
				2014/04/25	8.62			
				2013/11/16	10.22			

The cloud cover (%) of Sentinel 2 and Landsat were obtained from the metadata.
The cloud cover (%) of ALOS was obtained by image thresholding.

Table 3 Bands used for classification

Satellite & spatial resolution used for classification		sentinel-2		Landsat 8		Landsat5&ALOS	
Observation wavelength band	visible	4	MSI 10m	4	OLI 30m	3	AVNIR-2 10m
	near infrared	6		1		1	
	short wavelength infrared	3	MSI 20m	3		2	TM 30m
band usage total		13		8		6	

3. Satellite image preprocessing

3.1 Geometric correction

Satellite data cannot be directly superimposed on maps or other satellite data because it contains geometric distortion. The satellite images were geometrically corrected to compensate for this distortion. First, we selected six reference points from the bridge in the Monobe river basin. Second, satellite images were corrected using affine transformations (Equation 1) at an accuracy level of 0.5 pixels.

$$\begin{cases} x = au + bv + c \\ y = du + ev + f \end{cases} \tag{1}$$

a, b, c, d, e, f : *Conversion factor*
u, v : *before coordinate transformation*
x, y : *after coordinate transformation*

3.2 Normalization of luminance values

In this research, in order to correct the influence of the topography and the atmosphere, the brightness value was normalized using equation 2 [3]. Figure 4 is an example of this normalization for 2018/4/29 and 2017/4/4.

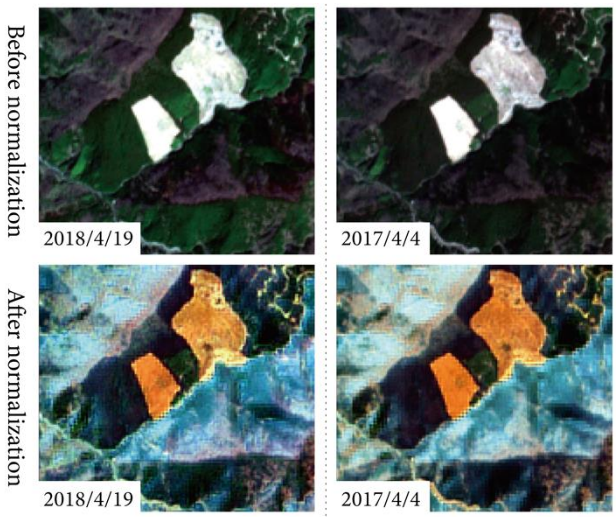

Figure 4 Normalization of luminance values

$$R_e(i) = \frac{N \times r_e(i)}{\sum_{i=1}^{N} r_e(i)} \tag{2}$$

R_e : *Normalized reflectance*
r_e : *Reflectivity*
N : *Total number of bands*
i : *Bandnumber*

4. Land cover classification by machine learning

4.1 Classification method

In this study, machine learning with supervised data was performed using a support vector machine (SVM) for land cover classification. The classification items were divided into six categories: deciduous broad-leaved trees, evergreen broad-leaved trees, evergreen conifers, mixed forests, bare land, and water areas. The classification results were accurately verified for each elevation. For the accuracy of land cover classification, we repeated to get supervised data with the goal of machine learning accuracy exceeding 80.0% in all areas. The classification procedure is shown in Figure 5.

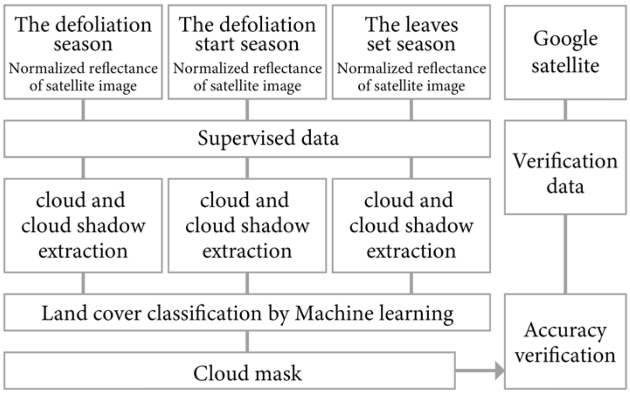

Figure 5 Classification procedure

4.2 Supervised data

In machine learning, it is necessary to obtain representative statistics that become the basis of each classification item. The representative statistic is called supervised data. The supervised data were obtained in four areas: Mt. Sanrei (elevation 2000 m), Matsuo pass (elevation 1000 m), Mt. Ookura (elevation 500 m), and the Saoka district (elevation 200 m), in order to consider the distribution pattern of vegetation by vertical distribution. In addition, the supervised data were obtained from pixels that did not contain clouds in the satellite images used for classification. Table 4 shows the number of pixels of the supervised data used for classification, which totaled 4500 pixels. The supervised data were obtained from the 2018 Sentinel-2 data. An RGB color image was created from bands 5, 6, and 7 of the satellite images of Sentinel-2 and the color changes of the three seasons (the defoliation start season, defoliation season, and leaf set season) were visually confirmed. The supervised data obtained three pixels or more from inside the boundary of vegetation. For bare land, the vegetation changed significantly due to logging; hence, pixels for bare land were acquired as supervised data in the fiscal years 2009 and 2018. The supervised data used for classification, except for the one in the fiscal year 2018, was acquired using the position coordinates installed by the image of fiscal year 2018.

Internet Journal of Society for Social Management Systems Vol.12 Issue 1 sms19-8001
ISSN: 2432-552X

Table 4 Number of pixels of supervised data used for classification

The Monobe River Basin

	Geographical Name	Mt.Sanrei	Matsuo pass	Mt.Ookura	Saoka district	Total number of supervised data
	altitude (m)	2000	1000	500	200	Number of pixels
Classification category	deciduous broad-leaved trees	200	500	0	0	700
	evergreen broad-leaved trees	0	0	500	500	1000
	evergreen conifers	200	500	500	500	1700
	mixed forests	200	500	0	0	700
	bare land	200				200
	water areas	200				200

4.3 Parameter settings

For SVM, it is necessary to set the amount of misclassification allowed in advance. Therefore, this study uses the cost parameter "C" and parameter "γ" of the RBF kernel to determine the complexity of the identification boundary. The effect of cost parameter C and parameter γ of the RBF kernel on machine learning is shown in Figure 6. In this study, the optimal parameters were determined by grid search using stratified k-fold cross-validation, which allows the number of divisions to be determined arbitrarily. The value of k was set to 5, where the variation in precision between the divisions was sufficiently reduced. Table 5 shows the selected parameters of each satellite.

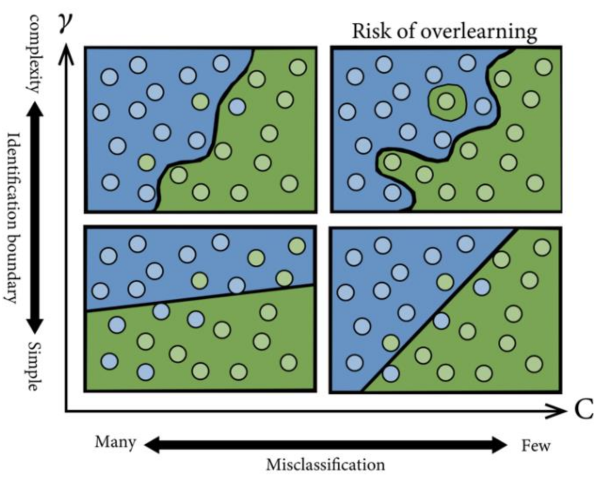

Figure 6 Cost parameter and RBF kernel parameter

Table 5 Parameters of each satellite

Satellite	Sentinel-2	Landsat 8	Landsat5 &ALOS
Machine learning method	SVM（Support Vector Machine）		
Parameter learning method	Grid earch using stratified k-fold CV		
kernel	RBF	RBF	RBF
C	100	100	100
γ	0.01	0.1	0.1

4.4 Cloud mask

Clouds and cloud shadows are not classified into six categories correctly when land cover classification is performed. Therefore, in order to solve this problem, the clouds and cloud shadows of the satellite images were extracted and overlaid on the classification result as a cloud mask. Clouds and cloud shadows extracted as supervised data of 200 pixels each from satellite images. In order to perform land cover classification, the supervised data acquired by six categories were set as "other than clouds and cloud shadows" and combined with supervised data of clouds and cloud shadows. Using a total of 1400 pixels of supervised data, SVM classified satellite images into three types: "clouds", "cloud shadows", "other than clouds and cloud shadows" (Figure 7).

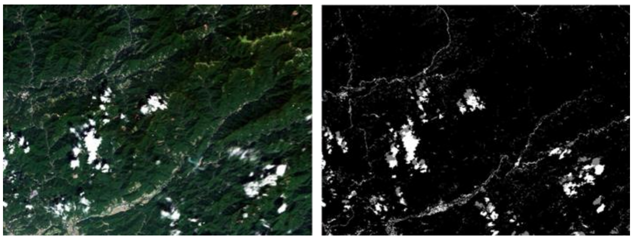

Figure 7 Cloud and cloud shadow extraction

4.5 Classification result

Classification results were obtained for a total of six years: Sentinel-2 for two years, Landsat 8 for three years, and Landsat5&ALOS for one year. The classification results for six years are shown in Figures 8 to 13. Between 2009 and 2018, mixed forest decreased, and bare land increased at the summit.

Internet Journal of Society for Social Management Systems Vol.12 Issue 1 sms19-8001
ISSN: 2432-552X

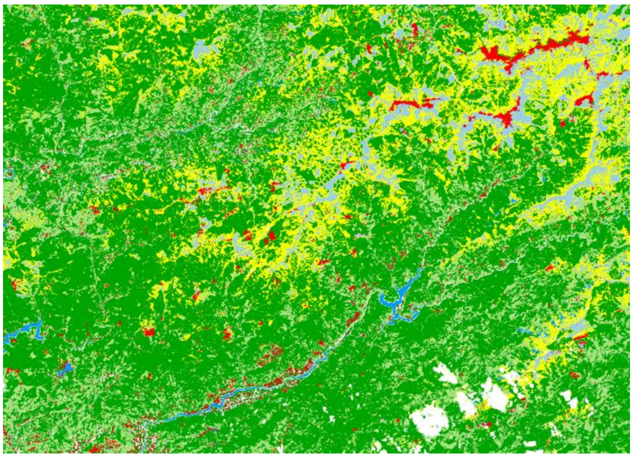

Figure 8 2018 classification result [Sentinel-2|MSI]

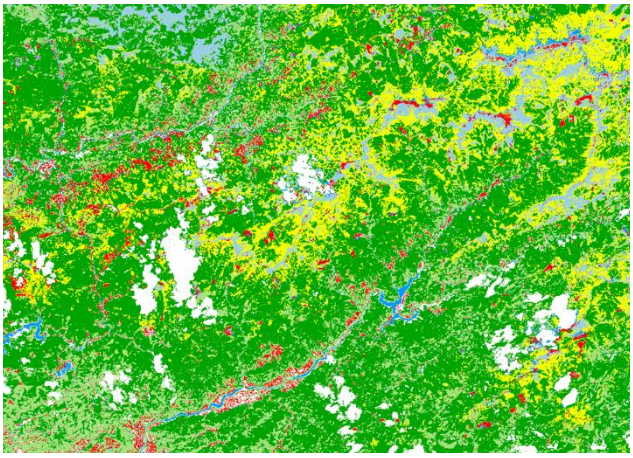

Figure 9 2017 classification result [Sentinel-2|MSI]

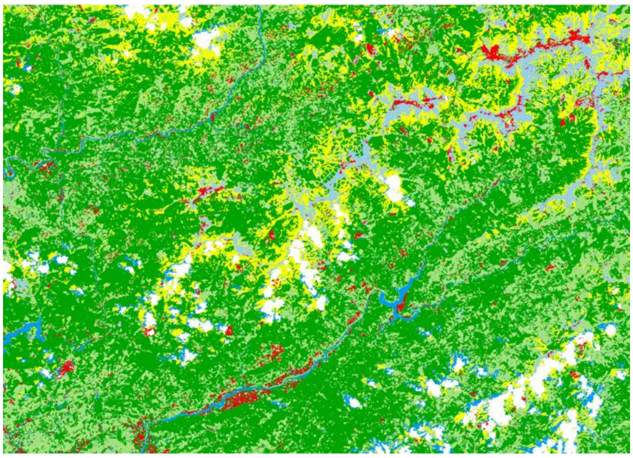

Figure 10 2016 classification result [Sentinel-2|MSI]

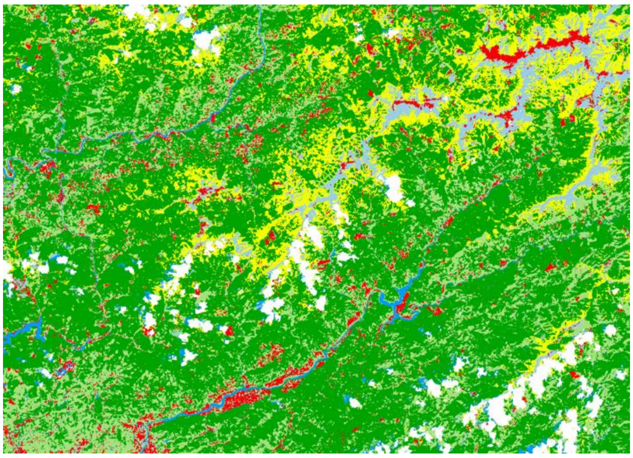

Figure 11 2015 classification result [Landsat8|OLI]

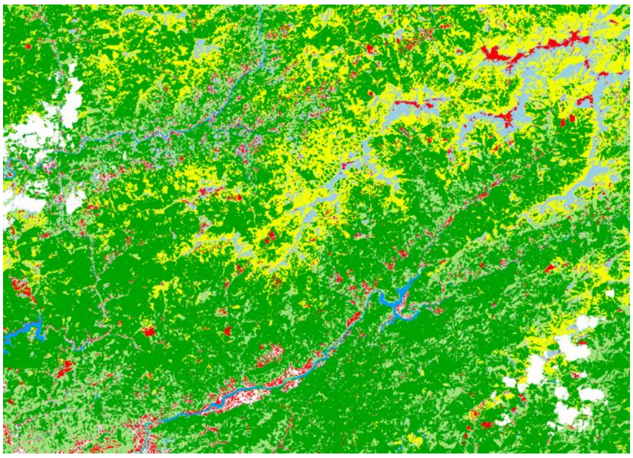

Figure 12 2014 classification result [Landsat8|OLI]

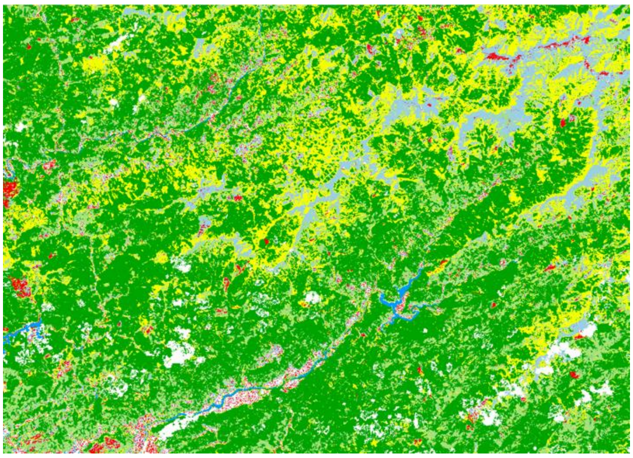

Figure 13 2009 classification result [Landsat5& ALOS|TM/AVNIR-2]

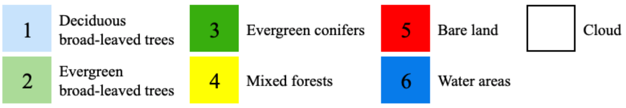

4.6 Accuracy verification

Verification data was acquired visually with Google satellite. In addition, verification data was taken as independent points of supervised data, and 50 pixels of each classification were acquired in Mt. Sanrei, Matsuo pass, Mt. Ookura, and the Saoka district. An accuracy verification was also performed. Table 6 shows the result of the accuracy verification in Matsuo pass in the fiscal year 2018, and Table 7 shows the overall accuracy in each fiscal year. The Matsuo pass, with a 1,000 m elevation above sea level, had lower accuracy compared to other areas owing to the complex vegetation. In addition, because the satellite image of Landsat 8 has a spatial resolution of 30 m, the accuracy is low at the mixed forest and the boundary of the vegetation, the overall accuracy is also low. Classification accuracy was improved by classification using Landsat5&ALOS.

Table 6 Accuracy verification result in Matsuo pass (FY 2018)

Sentinel-2 FY 2018 (Matuo pass)		Classification results: deciduous broad-leaved trees	evergreen broad-leaved trees	evergreen conifers	mixed forests	bare land	Total	Producer's accuracy (%)
Verification results	deciduous broad-leaved trees	36	2	0	12	0	50	72
	evergreen broad-leaved trees	0	0	0	0	0	0	0
	evergreen conifers	0	0	49	1	0	50	98
	mixed forests	2	0	1	47	0	50	94
	bare land	0	0	0	0	0	0	0
	Total	38	2	50	60	0	150	
User's accuracy (%)		94.7	0	98	78.3	0		88

5. Creation of vegetation change map

5.1 Noise elimination mask

Although classification results for six fiscal years were obtained, the classification results using only Landsat 8 have a spatial resolution of 30 m. Therefore, only the vegetation change maps from the three years where classification results had a 10 m spatial resolution (FY 2018, FY 2017, and FY 2009) were used.

Table 7 Overall accuracy results by elevation for each fiscal year

Artificial satellite		Sentinel-2		Landsat			Landsat5&ALOS
Classification fiscal year		2018	2017	2016	2015	2014	2009
Overall accuracy (%)	Mt.Sanrei	94	95.3	79.3	80.4	82	86.7
	Matsuo pass	88	87.3	78	80.7	80.7	82
	Mt.Ookura	99	99	81	81	85	89
	Saoka district	98	98	82	84.8	83	88

resolution. In this study, the vegetation change was classified into five categories according to its type, and later a vegetation change classification map was created. The five categories are: "changed in all three fiscal years", "changed from fiscal 2018", "changed from fiscal 2017", "no change in three fiscal years", and "changed only in fiscal 2017". Each satellite image has been geometrically corrected, but the positions of the satellite image pixels have slight deviations at each image. These slight deviations appear as vegetation change misclassification occurs near the boundary of different vegetation. Therefore, noise elimination mask processing was performed in consideration of the positional deviation of the boundary of vegetation. The vegetation change pattern map was divided into 3 by 3-pixel squares, and a boundary mask was formed according to how many corresponding pixels are included in nine pixels. In this case, when the pixel of "No change in three years" is within "six pixels or less", it is regarded as the boundary. The reason is that most of the boundaries are in contact with “no change in three years”. In addition, "All changes" and "Changed only in fiscal 2017" were also regarded as boundaries (Figure 14).

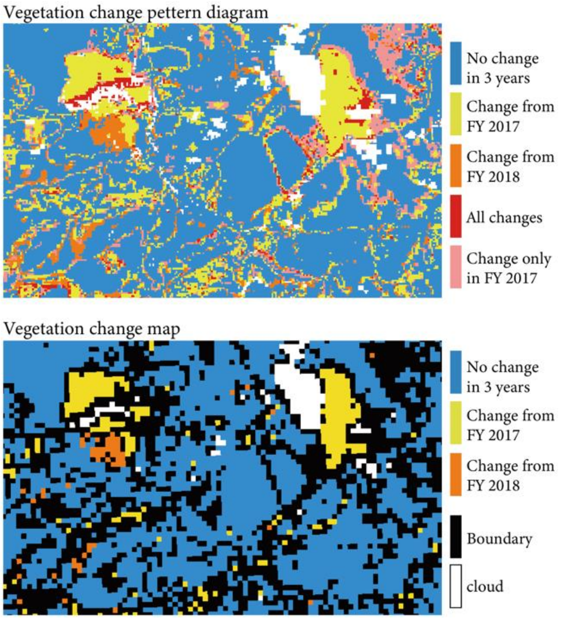

Figure 14 Noise elimination mask

5.2 Change extraction by vegetation change map

The study applied the cloud and noise elimination mask processing to the three patterns "No change in all three fiscal years", "changed from fiscal 2018", and "changed from fiscal 2017" to create a vegetation change map (Figure 15). This vegetation change map confirms that the evergreen conifer has changed to mixed forest in the three years around Yone, Otoyo-cho (Figure 16). In addition, in the area around Matsuo pass, observed that planted forests were logging and became bare land. Table 8 shows the change in vegetation from fiscal 2009 to 2017, and Table 9 shows the change in vegetation from fiscal 2017 to 2018 in pixels.

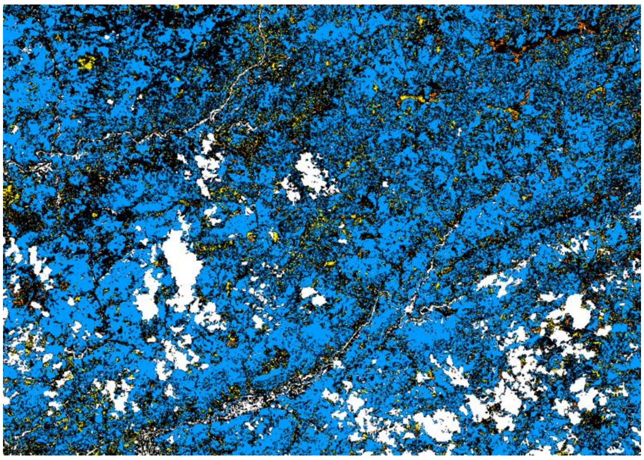

Figure 15 Vegetation change map

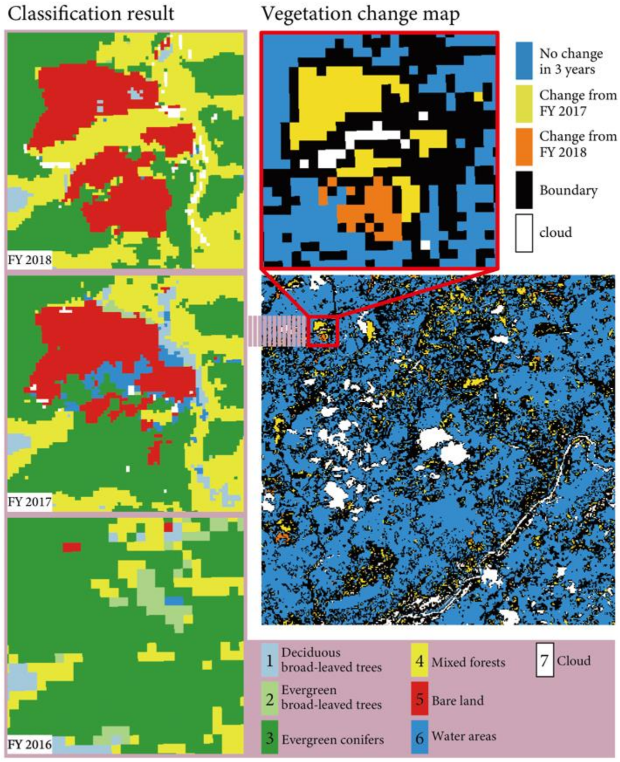

Figure 16 Vegetation change map in Yone, Otoyo-Cho

Table 8 Changes from fiscal 2009 to 2017

FY 2009 - 2017		fiscal 2017								
		deciduous broad-leaved trees	evergreen broad-leaved trees	evergreen conifers	mixed forests	bare land	water areas	cloud	boundary	Total
fiscal 2009	deciduous broad-leaved trees	16	10	25	2	1	0	0	0	54
	evergreen broad-leaved trees	7	310	183	13	1	0	0	0	514
	evergreen conifers	2	18	10723	25	0	3	0	0	10771
	mixed forests	93	39	3104	224	1	1	55	0	3517
	bare land	0	5	75	19	0	0	0	0	99
	water areas	0	0	1	0	0	0	0	0	1
	cloud	0	2	18	0	0	0	0	0	20
	boundary	0	0	0	0	0	0	0	11424	11424
	Total	118	384	14129	283	3	4	55	11424	26400

Table 9 Changes from fiscal 2017 to 2018

FY 2017 - 2018		fiscal year 2018								
		deciduous broad-leaved trees	evergreen broad-leaved trees	evergreen conifers	mixed forests	bare land	water areas	cloud	boundary	Total
fiscal year 2017	deciduous broad-leaved trees	18	6	2	92	0	0	1	0	119
	evergreen broad-leaved trees	0	371	12	1	0	0	0	0	384
	evergreen conifers	0	17	14042	47	0	11	12	0	14129
	mixed forests	0	23	49	211	0	0	0	0	283
	bare land	0	3	0	0	0	0	0	0	3
	water areas	0	1	3	0	0	0	0	0	4
	cloud	0	0	54	0	0	0	0	0	54
	boundary	0	0	0	0	0	0	0	11424	11424
	Total	18	421	14162	351	0	11	13	11424	26400

6. Vegetation restoration situation using the vegetation change map

6.1 Extraction of logging site

First, for investigating the situation of vegetation restoration, extraction of logging sites was carried out. As the extraction method, "the classification of fiscal 2009 was bare ground where the vegetation is recovered by the classification of fiscal 2018" was extracted. From there, 20 spots of logging sites were visually selected. The results are shown in Figure 17. The judgment of logging season was made by visual inspection based on the original image of Landsat 5, and confirmation of vegetation recovery was obtained from the classification result. The satellite images used to confirm the logging time are shown in Table 10.

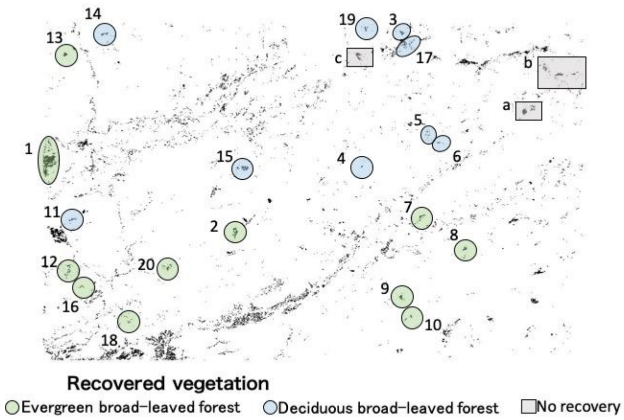

Figure 17 Logging site

Table 10 Satellite image used for confirmation of logging season

Landsat 5		
1996/12/3	2001/4/5	2006/4/3
1997/4/26	2002/3/7	2007/3/21
1998/5/31	2003/4/27	2008/5/26
1999/10/25	2004/3/28	
2000/3/1	2005/3/31	

6.2 Geographical features of logging sites

In order to know the geographical characteristics of the vegetation recovery situation of the deforested area, from the national land information download service, "altitude", “average inclination”, "soil" "geological features", "annual rainfall", “annual average temperature”, "irradiance", and "annual average global solar irradiance" was assigned (Table 11). We also expected some correlation between mean slope angle, soil, annual rainfall, and annual mean global radiation and vegetation recovery; however this correlation was not observed in this study. Conversely, there is a correlation between the elevation of the logging sites and the vegetation recovery period. This correlation is shown in Figure 18. It was found that there was a difference in the vegetation recovery around 800 m. The logging sites were restored to deciduous broad-leaved trees for elevations over 800 m. For elevations under 800 m, these sites were recovered to evergreen broad-leaved trees. Moreover, the forest restoration time increases with elevation. Additionally, there were several logging sites where recovery of vegetation did not occur even after 22 years. These logging sites correspond to a, b, and c in Figure 17. All these sites are located in the mountainous area, with elevations of more than 1,000 m. In terms of geology, for elevations over 800 m, there were three sites where the forest had recovered within 10 years, and the surface lithology at all these sites was phyllite. Conversely, many of these vegetation restoration sites were sandstone. In this study, vegetation restoration sites were found in 14 sandstone areas. Figure 19 shows the result of analyzing the correlation between the elevation of the sandstone area and the forest restoration period. The correlation coefficient was 0.824, showing a strong correlation.

Table 11 Geographic information of logging site

id	Vegetation recovery period (year)	Post-recovery vegetation	Altitude (m)	average inclination (angle)	soil	geological features	annual rainfall (mm)	annual average temperature (°C)	annual average global solar irradiance (MJm-2)
1	7	evergreen broad-leaved trees	396.7	18.3	brown forest soil	Phyllite	2593.6	13.1	12.9
2	17	evergreen broad-leaved trees	600.4	29.1	brown forest soil	Sandstone	3098.5	11.8	13.3
3	5	deciduous broad-leaved trees	829.5	26.8	dry brown forest soil	Phyllite	2196.8	9.7	12.9
4	17	deciduous broad-leaved trees	787.4	28.9	brown forest soil	Sandstone	2625.6	11.1	13
5	22	deciduous broad-leaved trees	1157.2	25.6	brown forest soil	Sandstone	2541	8.6	13.3
6	19	deciduous broad-leaved trees	1025.3	27.3	brown forest soil	Sandstone	2526.1	9.8	13.1
7	9	evergreen broad-leaved trees	652.1	32.5	dry brown forest soil	Sandstone	2687.3	12.2	13
8	12	evergreen broad-leaved trees	585.9	33.9	brown forest soil	Sandstone	2780.3	13.1	13
9	7	evergreen broad-leaved trees	426	29.7	brown forest soil	Sandstone	2844.8	12.4	13.6
10	10	evergreen broad-leaved trees	699.8	38.7	dry brown forest soil	Sandstone	2867.4	11.9	13.7
11	16	deciduous broad-leaved trees	820.9	24.7	damp brown forest soil	Sandstone	2921.4	11.7	13.5
12	8	evergreen broad-leaved trees	444.7	23.9	dry brown forest soil	Sandstone	3064.2	12.7	13.6
13	7	evergreen broad-leaved trees	496.6	29.2	brown forest soil	Black schist	2127.4	11.5	13
14	14	deciduous broad-leaved trees	811.4	30.1	brown forest soil	Black schist	1966.3	11	13.1
15	11	deciduous broad-leaved trees	879.7	26.6	brown forest soil	Sandstone	2886.7	9.8	13.4
16	11	evergreen broad-leaved trees	509.6	20.3	dry brown forest soil	Sandstone	3058	12.8	13.7
17	9	deciduous broad-leaved trees	801.6	20.4	dry brown forest soil	Phyllite	2248	11.4	12.6
18	7	evergreen broad-leaved trees	231.8	21.5	brown forest soil	Sandstone	2745.2	14.4	13.7
19	7	deciduous broad-leaved trees	948.2	22.6	brown forest soil	Phyllite	1995.7	10.2	12.9
20	14	evergreen broad-leaved trees	756.3	18.4	brown forest soil	Sandstone	2983.9	11.4	13.7

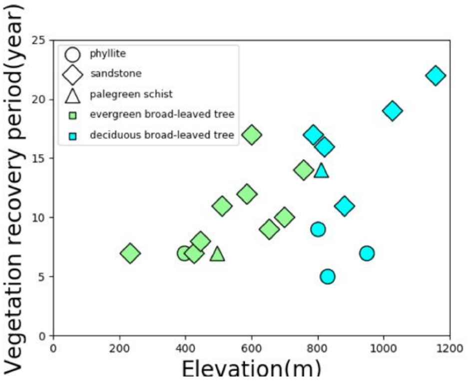

Figure 18 Elevation and vegetation recovery situation

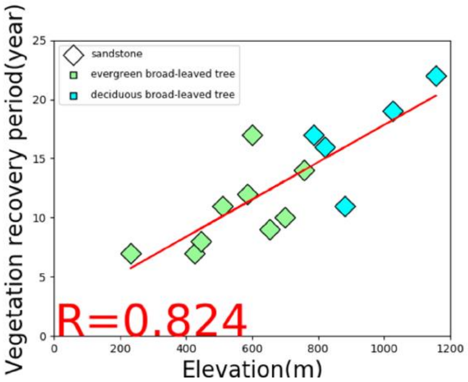

Figure 19 Elevation and vegetation recovery situation in the logging site where the surface geological features are sandstone

7. Conclusion

In this study, land cover classification was performed by machine learning using multiple satellites with different features. As a result, the land cover classification by Sentinel-2 was able to obtain 90.0% accuracy. Classification using Landsat 5 and ALOS achieved an accuracy of 80.0% or higher. These results show that for low observation band numbers, classification accuracy can be maintained by increasing the number of artificial satellites used. In addition, regarding the machine learning classification results, there was no significant difference in classification results even when using different satellite data. In this study, it became possible to predict vegetation recovery in the target area. In the verification process, a regression analysis of elevation and deforestation period was conducted for the vegetation recovery situation at the logging area. There was a correlation between vegetation recovery period and elevation of deciduous broad-leaved trees over 800 m or evergreen broad-leaved

ISSN: 2432-552X

trees under 800 m. Most of the vegetation recovery areas were composed of sandstone. It took 10 years to restore vegetation at an elevation of 500 m. There were some areas that could not be recovered at an elevation of 1000 m. This study showed that the recovery process or these areas would take around 18 years.

References

1) Japan Aerospace Exploration Agency (n.d.). How to make high resolution land use land cover map url: https://www.eorc.jaxa.jp/ALOS/alos-ori/index.html.

2) Masataka, T., 2012. *Fundamental of technology to measure the national land* JP: Japan Association of Surveyors

3) O. Akiko, F. Noboru and O. Atsuo. 2002. Suppression of Topographic and Atmospheric Effects by Normalizing the Radiation Spectrum of Landsat/TM by the Sum of Each Band. *Journal of The Remote Sensing Society of Japan*, 22(3):318-327.